



Ultrafast saturable absorption of large-diameter single-walled carbon nanotubes for passive mode locking in the mid-infrared

DAIKI OKAZAKI,¹  IKKI MORICHIKA,¹ HAYATO ARAI,² ESKO KAUPPINEN,³ QIANG ZHANG,³ ANTON ANISIMOV,⁴ ILKKA VARJOS,⁴ SHOHEI CHIASHI,² SHIGEO MARUYAMA,^{2,5}  AND SATOSHI ASHIHARA^{1,*} 

¹*Institute of Industrial Science, The University of Tokyo, 4-6-1, Komaba, Meguro-ku, Tokyo 153-8505, Japan*

²*Department of Mechanical Engineering, The University of Tokyo, 7-3-1, Hongo, Bunkyo-ku, Tokyo 113-8656, Japan*

³*Department of Applied Physics, Aalto University School of Science, 15100, FI-00076 Aalto, Finland*

⁴*Canatu, Ltd., Konalankuja 5, FI-00390 Helsinki, Finland*

⁵*Energy NanoEngineering Lab., National Institute of Advanced Industrial Science and Technology (AIST), Tsukuba 305-8564, Japan*

*ashihara@iis.u-tokyo.ac.jp

Abstract: We study the saturable absorption properties of single-walled carbon nanotubes (SWCNTs) with a large diameter of 2.2 nm and the corresponding exciton resonance at a wavelength of 2.4 μm . At resonant excitation, a large modulation depth of approximately 30 % and a small saturation fluence of a few tens of $\mu\text{J}/\text{cm}^2$ are evaluated. The temporal response is characterized by an instantaneous rise and a subpicosecond recovery. We also utilize the SWCNTs to realize sub-50 fs, self-start mode locking in a Cr:ZnS laser, revealing that the film thickness is an important parameter that affects the possible pulse energy and duration. The results prove that semiconductor SWCNTs with tailored diameters exceeding 2 nm are useful for passive mode locking in the mid-infrared range.

© 2020 Optical Society of America under the terms of the [OSA Open Access Publishing Agreement](#)

1. Introduction

Ultrafast lasers in the mid-infrared (mid-IR) range are attracting much attention because of their promising applications, represented by vibrational spectroscopy, material processing and strong-field phenomena. Their short temporal duration and broad spectrum spanning the molecular fingerprint region have brought about innovative advances in time-resolved spectroscopy [1], chemical reaction control [2,3], frequency comb spectroscopy [4,5] and spectroscopic nanoscale imaging [6,7]. Their high peak intensities localized in a fraction of time and location provide nonthermal polymer processing [8]. The relatively low frequency of mid-IR pulses provides large ponderomotive energy to enable better access of the extreme ultraviolet and soft X-ray regions in gaseous high-harmonic generation [9]. Recently, mid-IR pulses have also proven suitable for driving strong field phenomena in condensed matter without material damage [10–12]. Although frequency down conversion from $\text{Ti}^{3+}:\text{Al}_2\text{O}_3$ or $\text{Yb}^{3+}:\text{KGW}$ laser amplifiers may generate high-energy, few-cycle mid-IR pulses, alternative approaches based on direct mid-IR lasing are highly demanded in terms of simplicity, robustness, and energy efficiency.

There have been intensive studies on mode-locked lasers that generate ultrashort mid-IR pulses (e.g., Tm^{3+} -, Ho^{3+} -, and $\text{Tm}^{3+}/\text{Ho}^{3+}$ -doped solid-state and fiber lasers, Er^{3+} -, $\text{Ho}^{3+}/\text{Pr}^{3+}$ -, and Dy^{3+} -doped fluoride fiber lasers, and Cr^{2+} - and Fe^{2+} -doped II-VI chalcogenide solid-state lasers) [13]. Among them, $\text{Cr}^{2+}:\text{ZnS}/\text{ZnSe}$ lasers are especially promising for generating few-cycle

mid-IR pulses because of the outstanding spectroscopic properties of the gain materials [14]. Recent advances represented by few-cycle (15 fs) pulse generation with mega-watt peak power [15], laser diode pumping [16], and frequency comb operation [17,18] are making Cr:ZnS/ZnSe lasers the workhorse in ultrafast optical science.

Saturable absorbers (SAs) are essential in realizing stable and robust operation of passive mode locking. In fact, there have been several reports on the mode-locked oscillations of Cr:ZnS/ZnSe lasers using semiconductor saturable absorber mirrors (SESAMs) [19,20] and graphene [21–23]. In general, SESAMs exhibit a large modulation depth with a low saturation fluence, but their limited bandwidths tend to hamper few-cycle pulse generation. Graphene exhibits ideal properties of a large modulation depth, an ultrafast recovery, and a broad spectral response, but it is difficult to transfer graphene onto an optical window without defects or impurities.

Semiconductor single walled carbon nanotubes (SWCNTs) have been shown to exhibit superior saturable absorption properties at the S_{11} exciton resonance (transition from the 1st valence sub-band to the 1st conduction sub-band) [24–26]. They have been applied to laser mode locking at operating wavelengths below 2 μm in Yb-, Er-, and Tm:Ho-doped glass fiber lasers [24,26] and in some solid-state lasers [25,27]. Since the exciton resonance of a semiconductor SWCNT is determined by its chirality or diameter and lies at wavelengths shorter than 2 μm for the typical diameters of < 2 nm, semiconductor SWCNTs have rarely been used for mode locking at wavelengths longer than 2 μm . There has been an exception that mode locking was demonstrated at the wavelength of 2.4 μm by using SWCNTs with a diameter of 1.2-1.8 nm [28], but the details about how these SWCNTs worked as SAs at their non-resonant wavelengths are not clear.

Selective growth of SWCNTs with a certain mean diameter has been developed to locate the exciton resonance at wavelengths above 2 μm [29]. We have recently applied SWCNTs with a mean diameter of 2.2 nm and exciton resonance at 2.4 μm to self-start mode locking in a Cr:ZnS laser [30]. Their saturable absorption properties, however, have not yet been elucidated.

Here, we report investigations on the saturable absorption properties of large-diameter SWCNTs whose exciton resonance is located at the Cr:ZnS/ZnSe emission wavelength of 2.4 μm . By the open aperture Z-scan method and degenerate pump-probe absorption measurements, a small saturation fluence of tens of $\mu\text{J}/\text{cm}^2$ and subpicosecond recovery dynamics are characterized. These findings extend the past knowledge on the ultrafast photoresponse of semiconductor SWCNTs [31–34] to the mid-IR range. We also study the performance of a mode-locked Cr:ZnS laser using various thickness SWCNT film. It is found that an increased film thickness enables mode-locked operation with higher pulse energy and a shorter duration of sub-50 fs, which indicates a substantial impact of the film thickness on the laser performance. The presented results prove that diameter-controlled semiconductor SWCNTs with exciton resonance above 2 μm are useful for sub-50 fs, stable mode locking in the mid-IR range.

2. Sample preparation

SWCNTs are synthesized on nitrocellulose membrane filters through a floating catalyst CVD method [35,36]. The diameter is tailored so that the S_{11} transition is located at 2.4 μm by varying the CO_2 concentration, whereas the film thickness is controlled by varying the deposition time (see Refs. [29,37] for more details). Each of three films with different thicknesses is transferred onto a 2 mm thick CaF_2 substrate by a press transfer technique to fabricate a transmission-type SA as shown in Fig. 1(a). Here, we denote the thickest, medium thickness, and thinnest samples as Films 1, 2, and 3, respectively. The fabrication process described above enables simple and rapid transfer and therefore provides impurity-free, large-area SWCNT samples on arbitrary substrates.

The transmittance spectrum shown in Fig. 1(b) reveals the good compatibility between the S_{11} transition and the Cr:ZnS emission wavelength of approximately 2.4 μm . From the relationship between the S_{11} resonance frequency and the diameter [38], the mean diameter of our semiconductor SWCNTs is estimated to be 2.2 ± 0.3 nm. The broad absorption bandwidth of

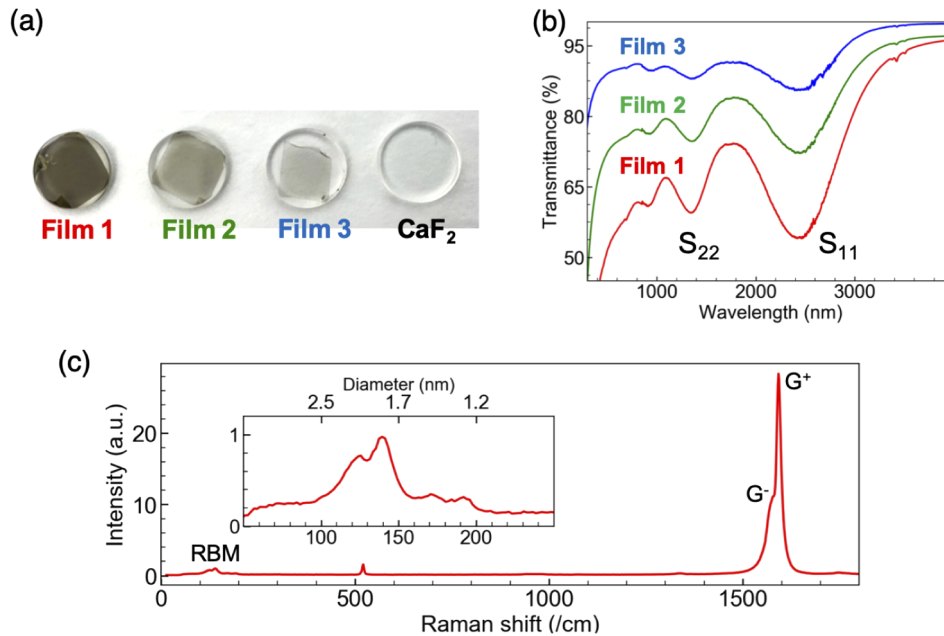


Fig. 1. (a) Picture of SWCNT films with various film thicknesses on CaF_2 substrates. (b) Transmission spectra of SWCNT films with different thicknesses. (c) Raman spectrum of Film 3. The inset shows a magnification of the RBM peak.

approximately 790 nm in FWHM, originating from the inhomogeneous distribution of diameters, is favorable for few-cycle pulse generation because it enables saturable absorption over a broad spectral range.

Figure 1(c) displays the Raman spectrum of Film 3 on a Si substrate measured with the excitation wavelength of 532 nm. The clear peaks of the tangential stretch modes, G^+ and G^- , indicate that no degradation is introduced throughout the synthesis and transfer processes [39]. It is known that the frequency of the radial breathing mode (RBM), ω_{RBM} (cm^{-1}), can be a measure of the tube diameter d (nm), described by an empirical relation $\omega_{\text{RBM}} = 248/d$ [40]. This relation tells the existence of the tubes with a diameter of > 2 nm from the components below 125 cm^{-1} shown in the inset of Fig. 1(c) (Note that the spectral shape is modified by the resonant enhancement effect).

3. Characterization of nonlinear absorption properties

3.1. Open aperture Z-scan measurement

The nonlinear absorption properties of the SWCNT films are measured by the open aperture Z-scan method. The light source is the home-built Cr:ZnS mode-locked laser described in Sect. 4, but with a different output coupler of 10 % transmission (instead of 2.5 %). It delivers linearly polarized pulses with a pulse energy of 2.1 nJ, a temporal duration of 50 fs, and a center wavelength of $2.3 \mu\text{m}$ at a 39.4 MHz repetition rate. The pulses are focused with a parabolic mirror ($f = 15$ mm) to a beam spot with a diameter of $42 \mu\text{m}$ and a corresponding focal depth of 0.6 mm. The transmitted power is measured by a thermal power meter while the sample position is scanned along the beam propagation direction. Then, the sample position is converted to optical fluence or pulse energy per area.

The optical transmittance at various input fluences is measured for Film 1, Film 2, and Film 3, as displayed in Fig. 2. It is clearly observed for each film that the transmittance T increases with

optical fluence from its initial value T_0 . The maximum value of the modulation depth $\Delta T/T_0$, where $\Delta T \equiv T - T_0$, is listed in Table 1. The modulation depth is found to increase with thickness by up to 29 %. This fact highlights the advantage of SWCNTs in that the available modulation depth is easily scalable with the film thickness.

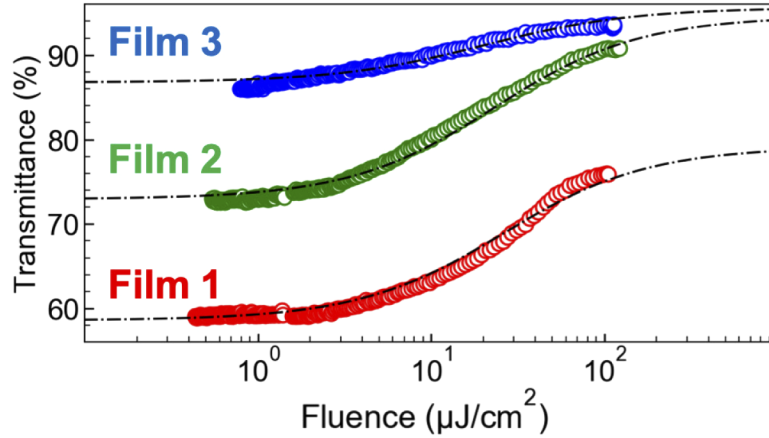


Fig. 2. Measured nonlinear transmission of the SWCNT films. The red, green and blue markers represent the data for Film 1, Film 2 and Film 3, respectively. The black lines are the numerical fittings.

Table 1. Summary of the properties of SWCNTs with various film thicknesses; T_0 – linear transmittance at 2.3 μm , $\Delta T/T_0$ – normalized transmittance change, $F_{\text{sat}}^{\text{eff}}$ – effective saturation fluence, E_p – maximum output pulse energy, $\Delta\lambda$ – maximum spectral FWHM of the laser output, τ – shortest pulse duration of the laser output.

Sample	T_0 (%)	$\Delta T/T_0$ (%)	$F_{\text{sat}}^{\text{eff}}$ ($\mu\text{J}/\text{cm}^2$)	E_p (nJ)	$\Delta\lambda$ (nm)	τ (fs)
Film 1	56	29	9.5	1.1	145	47.5
Film 2	74	25	14.9	0.59	113	57
Film 3	86	9.0	30.3	0.70	96	57

To estimate the saturation fluence F_{sat} , numerical fitting is performed by combining the Lambert-Beer law and the nonlinear absorption formula for a two level system as follows:

$$\frac{dF}{dz} = -\alpha F \quad (1)$$

$$\alpha(F) = \frac{\alpha_s}{1 + \frac{F}{F_{\text{sat}}}} + \alpha_{\text{ns}}. \quad (2)$$

Here, $\alpha(F)$, α_s and α_{ns} indicate the fluence-dependent, saturable, and nonsaturable absorption coefficients, respectively, F and F_{sat} denote the irradiated optical fluence and the saturation fluence of the sample, respectively, and z is the beam propagation direction along the film thickness. Here, we treat F_{sat} as a global parameter that is common to the three films. It is difficult to measure the absolute film thickness [41], but the relative thicknesses are estimated from the linear transmittance as 3.9 (Film 1), 2.1 (Film 2), and 1.0 (Film 3), which are used in the numerical integration.

The numerically estimated saturation fluence F_{sat} (the saturation peak intensity) of 18.6 $\mu\text{J}/\text{cm}^2$ (370 MW/cm^2) is similar to the values reported for thinner CNTs evaluated at their S_{11} resonance wavelengths of 1.3 μm and 1.9 μm [31,42]. Such small saturation fluence is beneficial for

realizing self-start mode locking because it induces meaningful loss modulation by the small intensity fluctuations appearing in continuous wave oscillations of multiple longitudinal modes. The deviation between the experimental data and numerical fittings may be due to the limitation of the two-level model; nonlinear transmission properties may also be affected by excited-state absorption and/or tube-tube interactions.

We may define an 'effective' saturation fluence $F_{\text{sat}}^{\text{eff}}$ with which a half of the saturable absorbance (or the normalized absorbance) $A_{\text{norm}}(F) = \log(T_0 + \Delta T)/\log T_0$ is saturated. As summarized in Table 1, $F_{\text{sat}}^{\text{eff}}$ increases with the film thickness. This is because more pulse energy is needed to saturate the absorption of the thicker film throughout its whole thickness.

3.2. Single-color pump-probe transmission spectroscopy

To investigate the temporal response of the nonlinear absorption, we perform single-color pump-probe spectroscopy on one of the SWCNT films (Film 1) by using the setup illustrated in Fig. 3(a). Here, we use linearly polarized (perpendicular to the plane of the paper), 1 kHz repetition rate, 100 fs pulses at the center wavelength of 2.3 μm generated from an optical parametric amplifier pumped by a Ti:Sapphire regenerative amplifier. The pulses are split into pump and probe pulses with an energy ratio of 12:1 by a wedged BaF₂ window with a wedged angle of 2°. The pump and probe pulses are focused by an off-axis parabolic mirror ($f = 76.2$ mm) and spatially overlap each other at the SWCNT film located at a defocused position. By rotating a half-wave plate, the excitation fluence is adjusted while the linear polarization direction is unchanged. The pump beam diameter is measured to be 380 $\mu\text{m} \times 310 \mu\text{m}$ at the sample. We measure the transmitted probe spectrum using a monochromator and a HgCdTe (MCT) detector array while scanning a translation stage. Then, the transmission change $\Delta T \equiv T - T_0$, where T and T_0 denote the probe transmittance with and without pumping, respectively, is measured as a function of the pump-probe delay time.

Figure 3(b) displays the spectrally resolved transmission change $\Delta T/T_0$ at various delay times measured for an excitation fluence of 56 $\mu\text{J}/\text{cm}^2$. Here, we note that this fluence is similar to the saturation fluence described in the last section and typical for SAs in mode-locked solid-state lasers. We see that the transmission change is spectrally homogeneous in its magnitude and temporal profile throughout the probe wavelengths. The slight difference in the delay time for the maximum transmission may come from the frequency chirp of the probe pulse and coherent artifacts. The top panel of Fig. 3(c) displays the kinetics of the spectrally integrated transmission change. It presents a sharp rise of saturable absorption or photobleaching (PB) followed by decay on a subpicosecond time scale. Here, this PB signal is naturally attributed to the space filling of the conduction band [43]. The following decay should reflect faster intraband relaxation and slower interband recombination [31,44]. Here, we note that there can be excess energy in the excitation process of SWCNTs with larger diameters or smaller S_{11} transmission frequencies, which causes intraband relaxation.

Figure 3(c) shows the temporal profiles of the spectrally integrated transmission changes for various excitation fluences of 17, 28, and 56 $\mu\text{J}/\text{cm}^2$. As the pump fluence increases, the peak value of the PB signal increases, with unchanged decay dynamics. The observed PB peak values are in reasonable agreement with the nonlinear transmission measurements presented in Fig. 2. Here we characterize the recovery dynamics by numerically fitting the data with a double exponential function,

$$\frac{\Delta T(t)}{T_0} = A_1 \exp\left(-\frac{t}{\tau_1}\right) + A_2 \exp\left(-\frac{t}{\tau_2}\right), \quad (3)$$

where t is the pump-probe delay time and τ_1 and τ_2 are time constants for the intraband and interband relaxation, respectively. A_1 and A_2 are the corresponding modulation amplitudes. By executing numerical fittings, τ_1 and τ_2 are evaluated to be 0.22 ps and 1.3 ps, respectively. A_1 is evaluated to be 9.4, 11, and 15 and A_2 is evaluated to be 6.2, 7.4, and 7.9 for excitation fluences

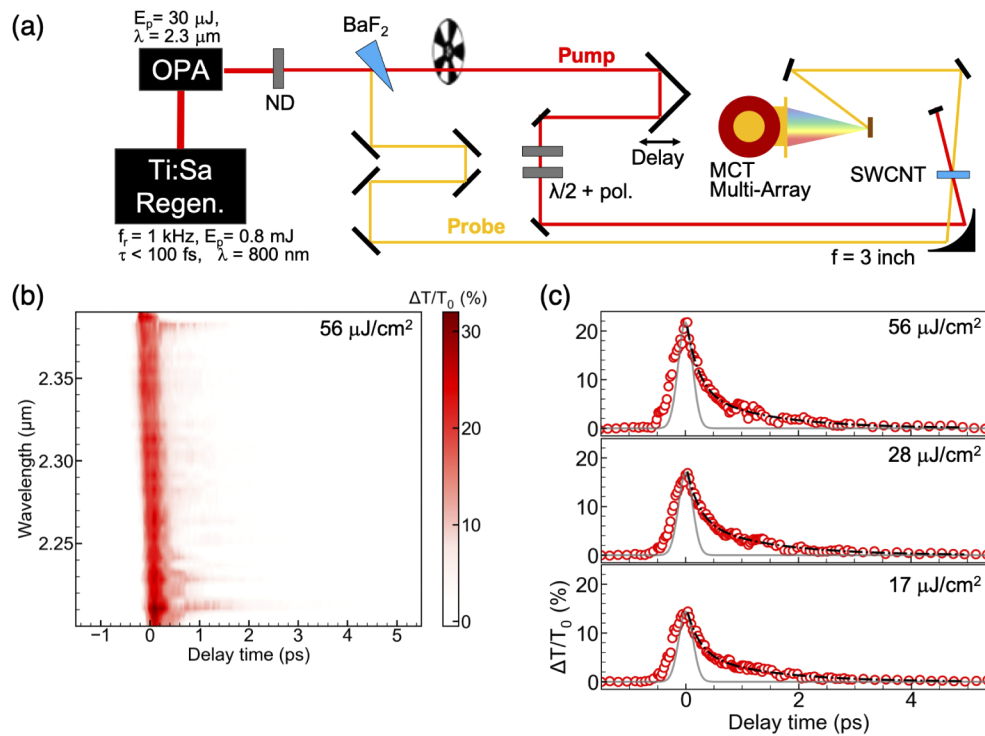


Fig. 3. (a) Schematic of the pump-probe transmission spectroscopy setup. Regen and OPA denote a regenerative amplifier and an optical parametric amplifier, respectively. Both the pump and probe pulses are linearly polarized (perpendicular to the plane of the paper). (b) Spectrally resolved signal of the normalized transmission change $\Delta T/T_0$ at various delay times measured for Film 1 under an excitation fluence of $56 \mu\text{J}/\text{cm}^2$. (c) Spectrally integrated transmission change (red markers) along with its numerical fitting (black line) and the instrumental function with an FWHM of 300 fs (grey line) for various excitation fluences.

of 17, 28 and $56 \mu\text{J}/\text{cm}^2$, respectively. Considering our time resolution of approximately 300 fs, estimated from a pump-probe absorption measurement on a Ge film, it is reasonable to take 0.22 ps as the upper limit of τ_1 , namely, $\tau_1 < 0.22$ ps. The evaluated time constants are similar to those reported for the SWCNTs that have S_{11} resonance in the near-infrared (near-IR) range [31,32,34,45]. It would be meaningful to note that the pump-probe transmission change turns to decrease when we increase further the pump fluence (above $100 \mu\text{J}/\text{cm}^2$), though its physical origin has not been clarified.

From a practical point of view, the spectrally broad feature, instantaneous rise, and fast decay on a picosecond time scale are all beneficial for mode locking and ultrashort pulse generation.

4. Cr:ZnS mode-locked oscillation properties

We investigate the mode-locked oscillation properties of a Cr:ZnS laser with SWCNT SAs of different film thicknesses. The experimental setup is shown in Fig. 4(a). The pump source, the cavity mirrors, and the tools for characterizing output pulses are almost the same as in our previous report [30], but there are some modifications, described as follows.

The Cr^{2+} concentration is increased to $6.3 \times 10^{18} \text{ cm}^{-3}$ for efficient absorption of the pump beam. The round-trip distance is increased to ~ 7.6 m, which leads to a repetition rate of 39.4 MHz as displayed in Fig. 4(b). The ratio of the long arm and the short arm is set to 5:2, and the

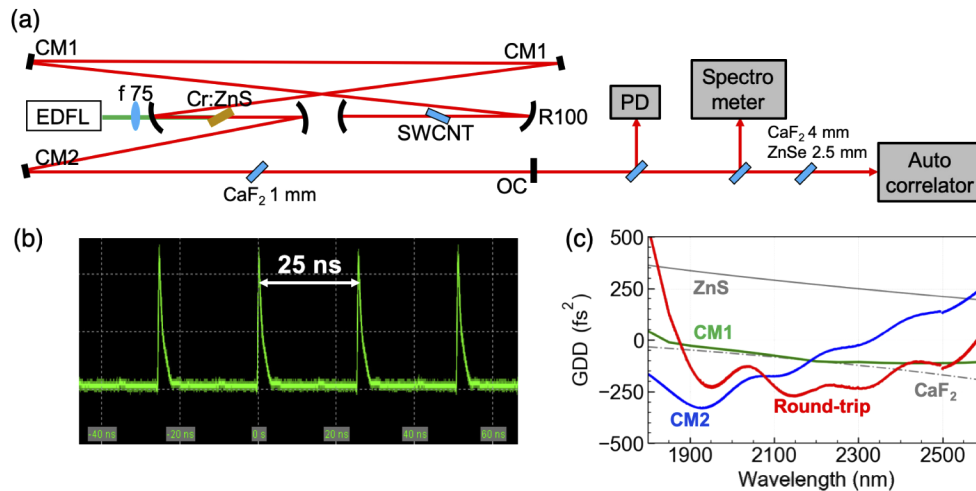


Fig. 4. (a) Schematic of the Z-fold optical cavity with the SWCNT SA. All of the concave mirrors are $f = 50$ mm. EDFL is an Er-doped fiber laser. The output properties are measured by a fast-MCT detector, a spectrometer, and a fringe-resolved autocorrelator [30]. A CaF_2 window and a ZnSe window are inserted in front of the autocorrelator for dispersion compensation. (b) Oscilloscope trace of the pulse train, which confirms the repetition rate of 39.4 MHz. (c) Calculated dispersion curves: the red curve represents the round-trip GDD, the green and blue curves represent GDD's per bounce of CM1 and CM2, respectively, and the solid grey curve and dotted grey curve represent GDD's of ZnS (1.9 mm) and CaF_2 (3 mm), respectively.

focusing mirrors for the SWCNT film are located at the end of the long arm. The calculated beam spot size of the cavity mode at the SWCNT film is approximately $100 \mu\text{m}$ in diameter. These modifications substantially reduce the mode-locking threshold as well as the lasing threshold for the same output coupler (OC) of 2.5% transmittance. In addition, two types of (instead of one) chirped mirrors (CM1 and CM2) are used in the current setup. Two CM1s are used for group delay dispersion (GDD) compensation, and a CM2 is used for third-order dispersion compensation. The GDD is further compensated by an inserted 1 mm thick CaF_2 plate. The resultant round-trip GDD is -220 fs^2 at a wavelength of $2.3 \mu\text{m}$. Figure 4(c) summarizes the wavelength dependence of GDD for each component and the round-trip GDD.

Figure 5(a) displays the output properties for SWCNT SAs with different film thicknesses. The oscillation regime is divided into four groups, i.e. cw oscillation (CW), Q-switched mode locking (QML), cw mode locking (CWML) and self-starting cw mode locking (SSML). QML states sometimes transition to CWML states under a small perturbation, and vice versa. A further increase in the pump power beyond the measured power range leads to an unstable pulse oscillation. We can see that the lasing threshold is higher for Film 1 than for others, which is due to the lower linear transmittance of Film 1. It is also found that the SSML state is sustained up to a higher pump power for Film 1 which should be related to the larger $F_{\text{sat}}^{\text{eff}}$ of Film 1 (see Table 1); a thicker film exhibits saturable absorption behavior up to higher fluence range.

Even if the oscillation gets unstable because of too much pumping, stable CWML or SSML with the same output power is recovered by decreasing the pump power to an original value. This reproducibility indicates that no damage happens on the SWCNT films. The maximum intracavity fluence at the SWCNT film evaluated as $290 \mu\text{J}/\text{cm}^2$ for Film 1, $155 \mu\text{J}/\text{cm}^2$ for Film 2, and $180 \mu\text{J}/\text{cm}^2$ for Film 3, gives lower limit of the damage threshold.

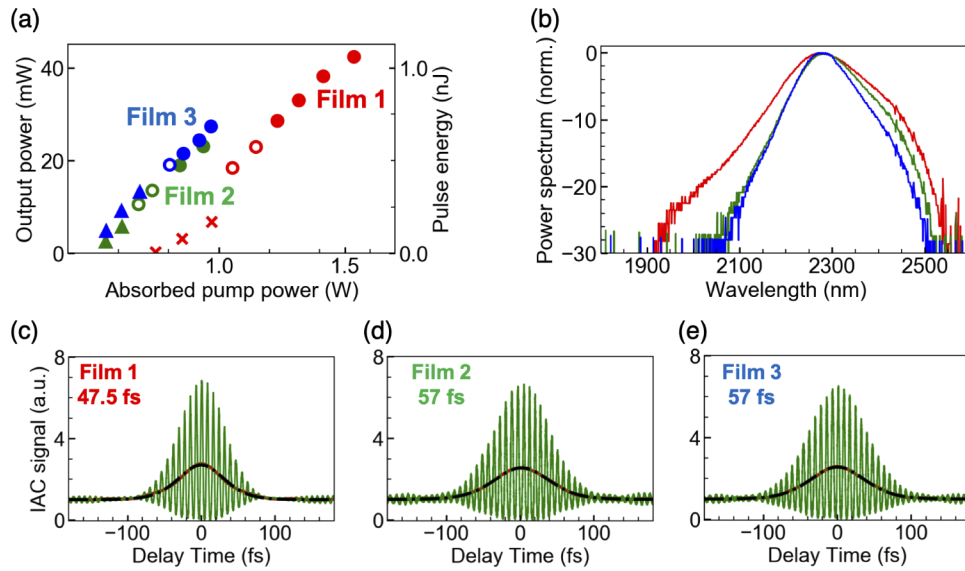


Fig. 5. Output properties of the Cr:ZnS laser using SWCNT films of different thicknesses: (a) pump power dependence of the output power, where \times , Δ , o , and \bullet represent cw oscillation, Q-switched mode locking, cw mode locking and self-start mode locking, respectively; (b) output power spectrum plotted in logarithmic scale (red: Film 1, green: Film 2, blue: Film 3); (c)–(e) measured interferometric autocorrelations (green), retrieved intensity autocorrelations (red), and their numerical fittings (black).

Figure 5(b) shows the power spectra of the output pulses for the different films, and Figs. 5(c)–5(e) show their fringe-resolved autocorrelation traces. Here, we optimize the pump power so that the pulse duration is minimized for each film (1.53, 0.94, and 0.97 W for Film 1, Film 2, and Film 3, respectively) while keeping the position of the SWCNT film unchanged. The spectral FWHM and the temporal duration of the output obtained with each film are summarized in Table 1. As is clearly seen, Film 1 gives the broadest pulse spectrum and the shortest pulse duration. The pulse spectrum spans a wavelength (frequency) range of 141 nm (8.2 THz) in FWHM and 310 nm (17.9 THz) at the -10 dB level. The pulse duration is estimated to be 47.5 fs (6.2 cycles at 2.3 μm) by assuming an ideal soliton shape. The time-bandwidth product is 0.387 which slightly deviates from the value of 0.315 for a Fourier-transform-limited soliton pulse. The deviation might come from imperfect GDD compensation or the finite relaxation time of the SWCNT SA.

The presented results indicate that the film thickness is an important parameter that affects the mode-locked laser performance. An increased film thickness provides, at the sacrifice of a low threshold, a larger possible modulation depth and stable SSML at a higher pulse energy, each of which in turn, contributes to a shortened pulse duration via direct pulse shortening and enhanced self-phase modulation, respectively.

5. Conclusion

We study the saturable absorption properties of large-diameter SWCNTs with exciton resonance at wavelengths beyond 2 μm . At the exciton resonance, the SWCNTs exhibit a large modulation depth as large as 30 % and a saturation fluence of a few tens of $\mu\text{m}^2/\text{cm}^2$. The temporal response is characterized by an instantaneous rise and a recovery with time constants of < 0.22 ps and 1.3 ps. These properties, together with a successful demonstration of self-starting mode locking in a

Cr:ZnS laser, prove that semiconductor SWCNTs with tailored diameters of > 2 nm are useful as ultrafast SAs in the mid-IR range. We also find that the film thickness is an important parameter because an increased film thickness provides a larger modulation depth and sustains stable mode locking up to a higher pump regime, enabling high-energy, shorter pulse generation.

The presented findings extend the past understanding of the photoresponse of SWCNTs to the mid-IR range and will stimulate further studies on engineering SWCNTs toward mid-IR applications and on high-energy, few-cycle mid-IR lasers.

Funding

Ministry of Education, Culture, Sports, Science and Technology (Q-LEAP JPMXS0118068681); Japan Society for the Promotion of Science (15H05760, 18H05329, 18K19030, 20H02651, 20J22067).

Disclosures

The authors declare no conflicts of interest.

References

1. P. Hamm and M. Zanni, *Concepts and methods of 2D infrared spectroscopy* (Cambridge University Press, 2011).
2. T. Stensitzki, Y. Yang, V. Kozich, A. A. Ahmed, F. Kössl, O. Kühn, and K. Heyne, "Acceleration of a ground-state reaction by selective femtosecond-infrared-laser-pulse excitation," *Nat. Chem.* **10**(2), 126–131 (2018).
3. I. Morichika, K. Murata, A. Sakurai, K. Ishii, and S. Ashihara, "Molecular ground-state dissociation in the condensed phase employing plasmonic field enhancement of chirped mid-infrared pulses," *Nat. Commun.* **10**(1), 3893 (2019).
4. F. Keilmann, C. Gohle, and R. Holzwarth, "Time-domain mid-infrared frequency-comb spectrometer," *Opt. Lett.* **29**(13), 1542–1544 (2004).
5. A. Schliesser, N. Picqué, and T. Hänsch, "Mid-infrared frequency combs," *Nat. Photonics* **6**(7), 440–449 (2012).
6. B. Markus, S. Albert, and F. Keilmann, "Spectroscopic near-field microscopy using frequency combs in the mid-infrared," *Opt. Express* **14**(23), 11222–11233 (2006).
7. E. A. Muller, B. Pollard, and M. B. Raschke, "Infrared chemical nano-imaging: Accessing structure, coupling, and dynamics on molecular length scales," *J. Phys. Chem. Lett.* **6**(7), 1275–1284 (2015).
8. K. Sugioka, "Progress in ultrafast laser processing and future prospects," *Nanophotonics* **6**(2), 393–413 (2017).
9. M. Lewenstein, P. Balcou, M. Ivanov, A. L'Huillier, and P. Corkum, "Theory of high-harmonic generation by low-frequency laser fields," *Phys. Rev. A* **49**(3), 2117–2132 (1994).
10. S. Ghimire, A. D. Dichiara, E. Sistrunk, P. Agostini, L. F. Dimauro, and D. A. Reis, "Observation of high-order harmonic generation in a bulk crystal," *Nat. Phys.* **7**(2), 138–141 (2011).
11. F. Kusa, K. Echternkamp, G. Herink, C. Ropers, and S. Ashihara, "Optical field emission from resonant gold nanorods driven by femtosecond mid-infrared pulses," *AIP Adv.* **5**(7), 077138 (2015).
12. K. Imasaka, T. Kaji, T. Shimura, and S. Ashihara, "Antenna-enhanced high harmonic generation in a wide-bandgap semiconductor ZnO," *Opt. Express* **26**(16), 21364–21374 (2018).
13. J. Ma, Z. Qin, G. Xie, L. Qian, and D. Tang, "Review of mid-infrared mode-locked laser sources in the 2.0 μm –3.5 μm spectral region," *Appl. Phys. Rev.* **6**(2), 021317 (2019).
14. I. T. Sorokina and E. Sorokin, "Femtosecond Cr²⁺-based lasers," *IEEE J. Sel. Top. Quantum Electron.* **21**(1), 273–291 (2015).
15. S. B. Mirov, I. S. Moskalev, S. Vasilyev, V. Smolski, V. V. Fedorov, D. Martyshkin, J. Peppers, M. Mirov, A. Dergachev, and V. Gapontsev, "Frontiers of mid-ir lasers based on transition metal doped chalcogenides," *IEEE J. Sel. Top. Quantum Electron.* **24**(5), 1–29 (2018).
16. N. Nagl, S. Gröbmeyer, V. Pervak, F. Krausz, O. Pronin, and K. F. Mak, "Directly diode-pumped, Kerr-lens mode-locked, few-cycle Cr:ZnSe oscillator," *Opt. Express* **27**(17), 24445–24454 (2019).
17. S. Vasilyev, I. Moskalev, V. Smolski, J. Peppers, M. Mirov, V. Fedorov, D. Martyshkin, S. Mirov, and V. Gapontsev, "Octave-spanning Cr:ZnS femtosecond laser with intrinsic nonlinear interferometry," *Optica* **6**(2), 126–127 (2019).
18. S. Vasilyev, V. Smolski, J. Peppers, I. Moskalev, M. Mirov, Y. Barnakov, S. Mirov, and V. Gapontsev, "Middle-IR frequency comb based on Cr:ZnS laser," *Opt. Express* **27**(24), 35079–35087 (2019).
19. I. T. Sorokina, E. Sorokin, and T. Carrig, "Femtosecond pulse generation from a SESAM mode-locked Cr:ZnSe laser," *Conf. on Lasers Electro-Optics/Quantum Electron. Laser Sci. Conf. Photonic Appl. Syst. Technol.* p. CMQ2 (2006).
20. E. Sorokin, N. Tolstik, K. I. Schaffers, and I. T. Sorokina, "Femtosecond SESAM-modelocked Cr:ZnS laser," *Opt. Express* **20**(27), 28947–28952 (2012).
21. M. N. Cizmeciyan, J. W. Kim, S. Bae, B. H. Hong, F. Rotermund, and A. Sennaroglu, "Graphene mode-locked femtosecond cr:znse laser at 2500 nm," *Opt. Lett.* **38**(3), 341–343 (2013).

22. N. Tolstik, E. Sorokin, and I. T. Sorokina, "Graphene mode-locked Cr:ZnS laser with 41 fs pulse duration," *Opt. Express* **22**(5), 5564–5571 (2014).
23. W. B. Cho, S. Y. Choi, C. Zhu, M. H. Kim, J. W. Kim, J. S. Kim, H. J. Park, D. H. Shin, M. Y. Jung, F. Wang, and F. Rotermund, "Graphene mode-locked femtosecond Cr²⁺:ZnS laser with ~300 nm tuning range," *Opt. Express* **24**(18), 20774–20780 (2016).
24. S. Kivistö, T. Hakulinen, A. Kaskela, B. Aitchison, D. P. Brown, A. G. Nasibulin, E. I. Kauppinen, A. Härkönen, and O. G. Okhotnikov, "Carbon nanotube films for ultrafast broadband technology," *Opt. Express* **17**(4), 2358–2363 (2009).
25. F. Rotermund, W. B. Cho, S. Y. Choi, I. H. Baek, J. H. Yim, S. Lee, A. Schmidt, G. Steinmeyer, U. Griebner, D. I. Yeom, K. Kim, and V. Petrov, "Mode-locking of solid-state lasers by single-walled carbon-nanotube based saturable absorbers," *Quantum Electron.* **42**(8), 663–670 (2012).
26. S. Yamashita, A. Martinez, and B. Xu, "Short pulse fiber lasers mode-locked by carbon nanotubes and graphene," *Opt. Fiber Technol.* **20**(6), 702–713 (2014).
27. G. Tanisali, I. Baylam, M. Tasci, J. E. Bae, F. Rotermund, U. Demirbas, and A. Sennaroglu, "21fs Cr:LiSAF laser mode locked with a single-walled carbon nanotube saturable absorber," *Opt. Lett.* **44**(19), 4662–4665 (2019).
28. N. Tolstik, O. Okhotnikov, E. Sorokin, and I. T. Sorokina, "Femtosecond Cr:ZnS laser at 2.35 μm mode-locked by carbon nanotubes," *Proc. SPIE* **8959**, 89591A (2014).
29. Y. Tian, M. Y. Timmermans, S. Kivistö, A. G. Nasibulin, Z. Zhu, H. Jiang, O. G. Okhotnikov, and E. I. Kauppinen, "Tailoring the diameter of single-walled carbon nanotubes for optical applications," *Nano Res.* **4**(8), 807–815 (2011).
30. D. Okazaki, H. Arai, A. Anisimov, E. I. Kauppinen, S. Chiashi, S. Maruyama, N. Saito, and S. Ashihara, "Self-starting mode-locked Cr:ZnS laser using single-walled carbon nanotubes with resonant absorption at 2.4 μm ," *Opt. Lett.* **44**(7), 1750–1753 (2019).
31. W. B. Cho, J. H. Yim, S. Y. Choi, S. Lee, A. Schmidt, G. Steinmeyer, U. Griebner, V. Petrov, D.-I. Yeom, K. Kim, and F. Rotermund, "Boosting the non linear optical response of carbon nanotube saturable absorbers for broadband mode-locking of bulk lasers," *Adv. Funct. Mater.* **20**(12), 1937–1943 (2010).
32. S. Xu, F. Wang, C. Zhu, Y. Meng, Y. Liu, W. Liu, J. Tang, K. Liu, G. Hu, R. C. T. Howe, T. Hasan, R. Zhang, Y. Shi, and Y. Xu, "Ultrafast nonlinear photoresponse of single-wall carbon nanotubes: a broadband degenerate investigation," *Nanoscale* **8**(17), 9304–9309 (2016).
33. G. Soavi, F. Scotognella, G. Lanzani, and G. Cerullo, "Ultrafast photophysics of single-walled carbon nanotubes," *Adv. Opt. Mater.* **4**(11), 1670–1688 (2016).
34. M. Chernysheva, R. Aleksey, F. Yuri, M. Chengbo, A. Raz, M. K. Sergey, M. D. Evgeny, and K. T. Sergei, "Carbon nanotubes for ultrafast fibre lasers," *Nanophotonics* **6**(1), 1–30 (2017).
35. A. Kaskela, A. G. Nasibulin, M. Y. Timmermans, B. Aitchison, A. Papadimitratos, Y. Tian, Z. Zhu, H. Jiang, D. P. Brown, A. Zakhidov, and E. I. Kauppinen, "Aerosol-synthesized swcnt networks with tunable conductivity and transparency by a dry transfer technique," *Nano Lett.* **10**(11), 4349–4355 (2010).
36. A. G. Nasibulin, A. Kaskela, K. Mustonen, A. S. Anisimov, V. Ruiz, S. Kivistö, S. Rackauskas, M. Y. Timmermans, M. Pudas, B. Aitchison, M. Kauppinen, D. P. Brown, O. G. Okhotnikov, and E. I. Kauppinen, "Multifunctional free-standing single-walled carbon nanotube films," *ACS Nano* **5**(4), 3214–3221 (2011).
37. Y. Liao, H. Jiang, N. Wei, P. Laiho, Q. Zhang, S. A. Khan, and E. I. Kauppinen, "Direct synthesis of colorful single-walled carbon nanotube thin films," *J. Am. Chem. Soc.* **140**(31), 9797–9800 (2018).
38. K. Liu, J. Deslippe, F. Xiao, R. B. Capaz, X. Hong, S. Aloni, A. Zettl, W. Wang, X. Bai, S. G. Louie, E. Wang, and F. Wang, "An atlas of carbon nanotube optical transitions," *Nat. Nanotechnol.* **7**(5), 325–329 (2012).
39. A. Jorio, M. Dresselhaus, R. Saito, and G. Dresselhaus, *Raman Spectroscopy in Graphene Related Systems* (Wiley, 2011).
40. A. Jorio, R. Saito, J. H. Hafner, C. M. Lieber, M. Hunter, T. McClure, G. Dresselhaus, and M. S. Dresselhaus, "Structural (n, m) determination of isolated single-wall carbon nanotubes by resonant raman scattering," *Phys. Rev. Lett.* **86**(6), 1118–1121 (2001).
41. S. Yoshida, Y. Feng, C. Delacou, T. Inoue, R. Xiang, R. Kometani, S. Chiashi, E. I. Kauppinen, and S. Maruyama, "Morphology dependence of the thermal transport properties of single-walled carbon nanotube thin films," *Nanotechnology* **28**(18), 185701 (2017).
42. J. Wang, X. Liang, G. Hu, Z. Zheng, S. Lin, D. Ouyang, X. Wu, P. Yan, S. Ruan, Z. Sun, and T. Hasan, "152 fs nanotube-mode-locked thulium-doped all-fiber laser," *Sci. Rep.* **6**(1), 28885 (2016).
43. J.-S. Lauret, C. Voisin, G. Cassabois, C. Delalande, P. Roussignol, O. Jost, and L. Capes, "Ultrafast carrier dynamics in single-wall carbon nanotubes," *Phys. Rev. Lett.* **90**(5), 057404 (2003).
44. G. N. Ostojic, S. Zaric, J. Kono, M. S. Strano, V. C. Moore, R. H. Hauge, and R. E. Smalley, "Interband recombination dynamics in resonantly excited single-walled carbon nanotubes," *Phys. Rev. Lett.* **92**(11), 117402 (2004).
45. E. A. Obraztsova, L. Lüer, E. D. Obraztsova, A. I. Chernov, D. Brida, D. Polli, and G. Lanzani, "Effect of environment on ultrafast photoexcitation kinetics in single-wall carbon nanotubes," *Phys. Status Solidi B* **247**(11-12), 2831–2834 (2010).